nanomaterials

MDPI

Article

DFT Study on the CO_2 Reduction to C_2 Chemicals Catalyzed by Fe and Co Clusters Supported on N-Doped Carbon

Qian Xue [1], Xueqiang Qi [1,2,*], Tingting Yang [1], Jinxia Jiang [3,*], Qi Zhou [1], Chuang Fu [1] and Na Yang [2,*]

[1] School of Chemistry and Chemical Engineering, Chongqing University of Technology, Chongqing 400054, China; xueq@stu.cqut.edu.cn (Q.X.); Tingty@stu.cqut.edu.cn (T.Y.); QiZhou@stu.cqut.edu.cn (Q.Z.); ChuangFu@stu.cqut.edu.cn (C.F.)
[2] Chongqing Key Laboratory of Chemical Process for Clean Energy and Resource Utilization, School of Chemistry and Chemical Engineering, Chongqing University, Chongqing 400044, China
[3] Chongqing Medical and Pharmaceutical College, Chongqing 400020, China
* Correspondence: xqqi@cqut.edu.cn (X.Q.); jiang106@cqu.edu.cn (J.J.); yna@cqu.edu.cn (N.Y.)

Abstract: The catalytic conversion of CO_2 to C_2 products through the CO_2 reduction reaction (CO_2RR) offers the possibility of preparing carbon-based fuels and valuable chemicals in a sustainable way. Herein, various Fe_n and Co_5 clusters are designed to screen out the good catalysts with reasonable stability, as well as high activity and selectivity for either C_2H_4 or CH_3CH_2OH generation through density functional theory (DFT) calculations. The binding energy and cohesive energy calculations show that both Fe_5 and Co_5 clusters can adsorb stably on the N-doped carbon (NC) with one metal atom anchored at the center of the defected hole via a classical MN_4 structure. The proposed reaction pathway demonstrates that the Fe_5-NC cluster has better activity than Co_5-NC, since the carbon–carbon coupling reaction is the potential determining step (PDS), and the free energy change is 0.22 eV lower in the Fe_5-NC cluster than that in Co_5-NC. However, Co_5-NC shows a better selectivity towards C_2H_4 since the hydrogenation of CH_2CHO to CH_3CHO becomes the PDS, and the free energy change is 1.08 eV, which is 0.07 eV higher than that in the C-C coupling step. The larger discrepancy of d band center and density of states (DOS) between the topmost Fe and sub-layer Fe may account for the lower free energy change in the C-C coupling reaction. Our theoretical insights propose an explicit indication for designing new catalysts based on the transition metal (TM) clusters supported on N-doped carbon for multi-hydrocarbon synthesis through systematically analyzing the stability of the metal clusters, the electronic structure of the critical intermediates and the energy profiles during the CO_2RR.

Keywords: DFT; CO_2RR; clusters; selectivity and activity

Citation: Xue, Q.; Qi, X.; Yang, T.; Jiang, J.; Zhou, Q.; Fu, C.; Yang, N. DFT Study on the CO_2 Reduction to C_2 Chemicals Catalyzed by Fe and Co Clusters Supported on N-Doped Carbon. *Nanomaterials* **2022**, *12*, 2239. https://doi.org/10.3390/nano12132239

Academic Editor: Gregory M. Odegard

Received: 14 May 2022
Accepted: 25 June 2022
Published: 29 June 2022

1. Introduction

The electrochemical CO_2 reduction reaction (CO_2RR), as a useful method to convert CO_2 into value-added chemical products, which not only helps to solve the energy and environmental problems caused by fossil fuel combustion but also achieves sustainable development [1–4]. The main products of CO_2RR are generally divided into C_1 products (e.g., CO, CH_4, CH_3OH, HCOOH, etc.) [5] and C_2 products (e.g., C_2H_4, C_2H_5OH, CH_3COOH, etc.) [6]. Cu and Cu-derived materials have been considered the most common electrocatalysts for the CO_2RR in the early stages [7,8]. Furthermore, Ag-based [9,10] and Au-based [11–13] catalysts can selectively reduce CO_2 to CO at low overpotentials. However, they suffer from low utilization of metal atoms and a low C_{2+} selectivity.

Recently, the single-atom catalysts (SACs) of metal loaded on carbon substrates (metal nitrogen-doped carbon-based catalysts) have become a rather hot frontier for the maximized atom utilization efficiency and defined active centers. Rossmeisl et al. [14,15] found that the transition metal nitrogen-doped carbon-based catalysts (M-N-C, M = Mn, Fe, Co, Ni or Cu) performed a high CO selectivity for CO_2RR. Furthermore, both Mn-N-C and Fe-N-C

also possessed CO selectivity as well as trace amounts of CH_4, which was assigned to the stronger CO binding of the Fe and Mn porphyrine-like structures. Zu et al. [16] successfully synthesized atomically dispersed Sn sites on nitrogen-doped carbon, which performs excellent activity and stability for formate generation at a kilogram scale with a quick freeze-vacuum drying-calcination method. Many Ni-based, Fe-based and Co-based SACs have exhibited high electrocatalytic activity and Faradaic effectivity (FE) for the CO_2RR with CO as the primary product due to the moderate adsorption energies of *COOH and *CO intermediates, as well as the high activation barrier for the hydrogen evolution reaction (HER) [17,18].

Though the widespread study on the single-atom catalysts enhanced the utilization efficiency of metal atoms, most of the current studies are limited to the reduction of CO_2 to C_1 products. Compared to C_1 products, C_{2+} products have a higher economic and chemical utilization value [19–21]. Cu-based SACs, up to now, have still performed good electrochemical reduction of CO_2 to C_{2+} chemicals [22,23]. However, Karapinar [24] revealed that the atomically dispersed CuN_x sites could reversibly convert into Cu clusters during CO_2RR, which are suggested as the real multiple active sites for CH_3CH_2OH production. Considering the fact that a single metal atom can accommodate only a single CO, it is difficult to activate two CO_2 molecules simultaneously to trigger the C-C coupling reaction based on an isolated metal center. Thus C-C coupling proceeding on the single metal atoms is quite difficult. Therefore, the catalysts with multiple active sites need to be considered to achieve the conversion from CO_2 to C_2 products [25].

Transition metal (TM) clusters with precise atomic numbers can offer multiple active sites, tune the size-dependent catalytic activity [26], and allow them to find the highest reactivity for the activation and dissociation of strong chemical bonds from CO_2. Xu et al. [27] reported a facile underpotential deposition technique to fabricate Cu clusters on carbonaceous substrates via rationally introducing S dopants in graphite foam. The obtained free-standing electrode exhibited high activity and excellent long-term stability toward oxygen reduction reaction. Pei et al. [28] found the trimeric metal clusters anchored on N-doped porous graphitic sheets possess a good selectivity and superiority towards CO_2RR to multi-carbon products due to the multiple active sites.

Considering the loading of metal clusters with a precise number of atoms on the active substrate can not only avoid the problem of low stability of bare metal cluster catalysts at room temperature but also further enhance their stability and catalytic efficiency. Graphite-based materials are currently widely used as substrates for electrocatalysts. To access C_2 products more efficiently, herein, we employed density functional theory (DFT) calculations to explore the CO_2RR catalyzed by Fe_n (n = 1, 3–5) anchoring on N-doped carbon (Fe_n-NC) to C_2H_4 and C_2H_5OH in this work. Furthermore, the Co_5 cluster supported on N-doped carbon (Co_5-NC) was explored comparatively. We found that Fe_5 loaded on NC exhibit significant activity for promoting the reduction of CO_2 to C_2 products, while the Co_5 cluster has higher priority for the selective synthesis of C_2H_4. Our findings provide insights into the design of highly active catalysts for CO_2RR and create a platform for developing metal cluster-NC electrocatalysts.

2. Theoretical Method

First principle calculations were performed using DFT with spin polarization utilizing the Vienna Ab initio Simulation Package (VASP). The projected augmented wave (PAW) [29–31] was used, and the generalized gradient approximation (GGA) realized by the Perdew–Burke–Ernzerhof function (PBE) was adopted to incorporate the exchange-correction functional [32]. A 2 × 2 × 1 Monkhorst-Pack K-point was sampled in the Brillouin zone, and a cut-off energy of 500 eV was set for geometric optimization. The convergence criteria are of 10^{-5} eV in energy between two electronic iteration steps and

0.02 eV/Å in force for every atom [33]. Our calculations of catalytic performance are based on the computational hydrogen electrode (CHE) proposed by Nørskov et al. [34]:

$$H^+_{(aq)} + e^- \rightarrow \frac{1}{2}H_2(g) \quad (1)$$

The change of the free energy for the step $*A + H^+ + e^- \rightarrow *AH$ can be equal to the reaction: $*A + \frac{1}{2}H_2(g) \rightarrow *AH$ at 0 V versus the reversible hydrogen electrode (RHE) at all pH values.

We employ five types of small iron clusters Fe_n (n = 1, 3–5) supported on nitrogen-doped carbon sheets as the calculation models. The defects of *NC* provide ideal anchor sites for the iron cluster. To estimate the stability of supported TM clusters, the binding energy (E_b) of TM_n cluster on *NC* is calculated by Equation (2)

$$E_b = E_{TM_n-NC} - E_{TM_n} - E_{NC} \quad (2)$$

Here E_{TM_n-NC} is the total energy of the optimized TM_n cluster supported on *NC*. The terms E_{TM_n} and E_{NC} refer to the energies of isolated TM_n cluster and support. We calculated the cohesive energy (E_c) of each TM_n cluster to further evaluate the stability of TM_n-*NC* catalysts, with E_c defined as:

$$E_c = (E_{cluster} - nE_{TM})/n \quad (3)$$

Here the $E_{cluster}$ and E_{TM} represent the energy of the total energy of the TM_n cluster and the energy of single *TM* atom; n is the number of TM atoms in the cluster. The more negative cohesive energy (E_c) indicates a more stable structure.

The adsorption energy (E_{ads}) of every intermediate species is defined by Equation (4)

$$E_{ads} = E_{C_xH_yO_z-TM_n-NC} - E_{TM_n-NC} - E_{C_xH_yO_z} \quad (4)$$

where $E_{C_xH_yO_z-TM_n-NC}$ refers to the total energy of the adsorbed species on the supported TM_n cluster, and E_{TM_n-NC} is the energy of supported TM_n cluster. $E_{C_xH_yO_z}$ refers to the energies of $C_xH_yO_z$ in gas phase, respectively. The more negative adsorption energy indicates a stronger binding between *TM* cluster and *NC* support. Gibbs free energy change (ΔG) [35,36] is defined as:

$$\Delta G = \Delta E + \Delta E_{ZPE} + \Delta \int C_P dT - T\Delta S + \Delta G_{pH} + \Delta G_U \quad (5)$$

where ΔE, ΔE_{ZPE}, $\Delta \int C_P dT$ and ΔS are the total energy difference, the zero-point energy difference, the difference in enthalpic correction and the entropy change between the products and reactants obtained from DFT calculations, respectively. The zero-point energies (*ZPE*) and total entropies of the gas phase were computed from the vibrational frequencies, and the vibrational frequencies of the adsorbed species were also computed to obtain the *ZPE* contribution to the free energy expression. Only vibrational modes of the adsorbates were computed explicitly, while the catalyst sheet was fixed (assuming that vibration contribution to the free energy from the substrate is negligible) [37,38]. T is the temperature (298.15 K). The influence of applied potential is: $\Delta G_U = -neU$, where U is the external potential versus RHE, e is the electron transfer, and n is the number of proton–electron pairs. ΔG_{pH} is the free energy correction due to the concentration of H^+. $\Delta G_{pH} = -k_BT \times \ln[H^+] = k_BT \times \ln 10 \times pH$, where k_B is the Boltzmann constant, and the value of pH was assumed to be zero for acidic conditions.

3. Results and Discussion

3.1. The STABILITY Analysis of Fe_n-NC

For the Fe_n clusters supported on the NC substrate (Fe_n-NC), n = 1, 3, 4 and 5 were chosen to be studied here since the Fe_2 cluster is unstable [39]. As shown in Figure 1,

for the adsorption of a single Fe atom on the NC substrate (Figure 1a), the mono Fe atom coordinated with the four nitrogen atoms and Fe-NC maintains a perfect monolayer structure, which is in agreement with previous results [40]. For the adsorption of Fe_n clusters with n ranging from 3 to 5 (Figure 1b–d), one Fe atom is anchored at the same position with that in a single Fe atom. Two Fe atoms bound to the doped nitrogen atoms with distances of about 2.1~2.3 Å, respectively, while the other Fe atoms bound together through Fe-Fe metal bonds.

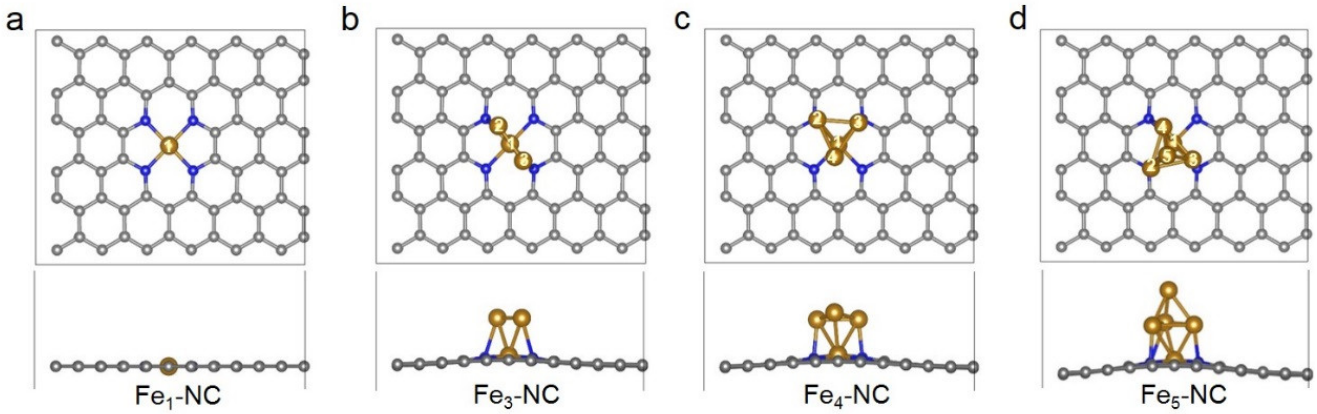

Figure 1. Top-view and side-view of optimized structures of Fe_1 (**a**), Fe_3 (**b**), Fe_4 (**c**) and Fe_5 (**d**) clusters supported on four nitrogen-doped carbon. The gold, blue and gray spheres represent Fe, N and C atoms, respectively. The different Fe sites are marked with white numbers.

As listed in Table 1, all the binding energies of Fe_n clusters on NC supports are thermodynamically favorable ($E_b < 0$). With the increase in Fe atoms, the binding energy decreases except for the magic Fe_5 cluster, which means that the small Fe clusters may tend to aggregate from small clusters to bigger clusters on NC support. The reason for the decreased binding energy of the magic Fe_5 cluster lies in that the Fe^{5site} located at the top site, as shown in Figure 1d. Hence there is no interaction with the NC support. What is more, the cohesive energy of various Fe_n clusters was also explored according to Equation (3), as shown in Table 1. It can be found that with the increase in Fe atoms in the cluster, the cohesive energy becomes thermodynamically favorable.

Table 1. The Bader charge of Fe atom in various Fe_n-NC, binding energies (E_b) between the Fe_n cluster and NC, and the cohesive energy (E_c) of Fe atoms in various Fe_n clusters.

Catalyst	* Bader Charge (e)					E_b (eV)	E_c (eV)
	Fe ^{1site}	Fe ^{2site}	Fe ^{3site}	Fe ^{4site}	Fe ^{5site}		
Fe_1-NC	−1.07	-	-	-	-	−9.01	0
Fe_3-NC	−0.80	−0.32	−0.31	-	-	−9.73	−0.35
Fe_4-NC	−0.81	−0.34	−0.33	−0.19	-	−9.79	−0.62
Fe_5-NC	−0.81	−0.36	−0.35	−0.28	−0.01	−8.34	−1.01

* negative Bader charge means electron loss.

3.2. Electrocatalytic CO_2RR

The charge difference between two active transition atoms plays a key role during CO_2RR, and the mixed oxidation state of the catalytic centers can boost the C-C coupling [41,42]. Thus the Bader charges of various Fe clusters adsorbed on NC were investigated. As listed in Table 1, one can find that the electrons can transfer from the clusters to the support, making the whole Fe cluster positively charged, and each Fe atom in the cluster is positively charged as well. Herein, the Fe_n clusters are favorable to the CO_2RR; thus the electron-accepting properties of the positively charged Fe and Co sites are favorable for stabilizing the CO_2RR intermediates [43]. The largest charge transfer can be determined for

the single Fe atom configuration since the monatomic Fe interacts with four coordinated N atoms. Furthermore, significant discrepancies for each charged Fe atom in the Fe_3, Fe_4 and Fe_5 clusters can be determined, which is beneficial for the C-C coupling reaction.

The conversion of CO_2 to CO catalyzed by various Fe_n clusters was calculated, as shown in Figure 2; the PDS is the *CO to CO for all the Fe_n-NC with a maximum Gibbs free energy ($\Delta G_3 = \Delta G_{CO} - \Delta G_{*CO}$). The ΔG_3 are 0.91, 1.14 and 1.58 eV for the Fe-NC, Fe_3-NC and Fe_4-NC, respectively. This value increases to 1.94 and 2.29 eV at two different sites of Fe_5-NC. Thus it can be deemed that the Fe-NC, Fe_3-NC and Fe_4-NC require a lower overpotential to drive the desorption of CO, indicating that these structures favor the conversion of CO_2 to CO. The $*CO \rightarrow CO(g)$ step with strong *CO binding leads to a positive ΔG of CO desorption. The relatively strong binding of *CO on Fe-N_x is fully supported by the experimentally confirmed exclusive ability of the Fe-N_x catalyst to produce the hydrocarbon CH_4 [44].

In simple terms, one could say that to produce subsequent reaction products from CO during the CO_2RR; the CO molecule must be bound strong and long enough to undergo subsequent dissociation and hydrogenation steps to arrive at CH_4 or other small organic molecules. Herein, our work focuses on the reduction of CO_2 to C_2 products, which requires improved selectivity and activity by inhibiting the unwanted, i.e., C_1 hydrocarbon reaction pathway, which favors both the stabilization of *CO on the catalyst surface and the formation of C-C bonds. The strongest interaction for CO on the two Fe_5-NC sites means that CO does not leave the iron cluster surface easily, which, in turn, favors the subsequent C_2 product conversion. Therefore, the following study focuses on the performance of electrocatalytic CO_2 reduction to C_2H_4 and CH_3CH_2OH over the Fe_5-NC cluster. In order to further extend this result to other systems, the Co_5 cluster supported on NC was chosen to be studied comparatively (Figure S1). As shown in Table 2, the E_b value between the Co_5 cluster and the NC is −10.00 eV, and the E_c value of the Co atom is −1.39 eV, which means the Co_5 cluster can adsorb stably on the NC.

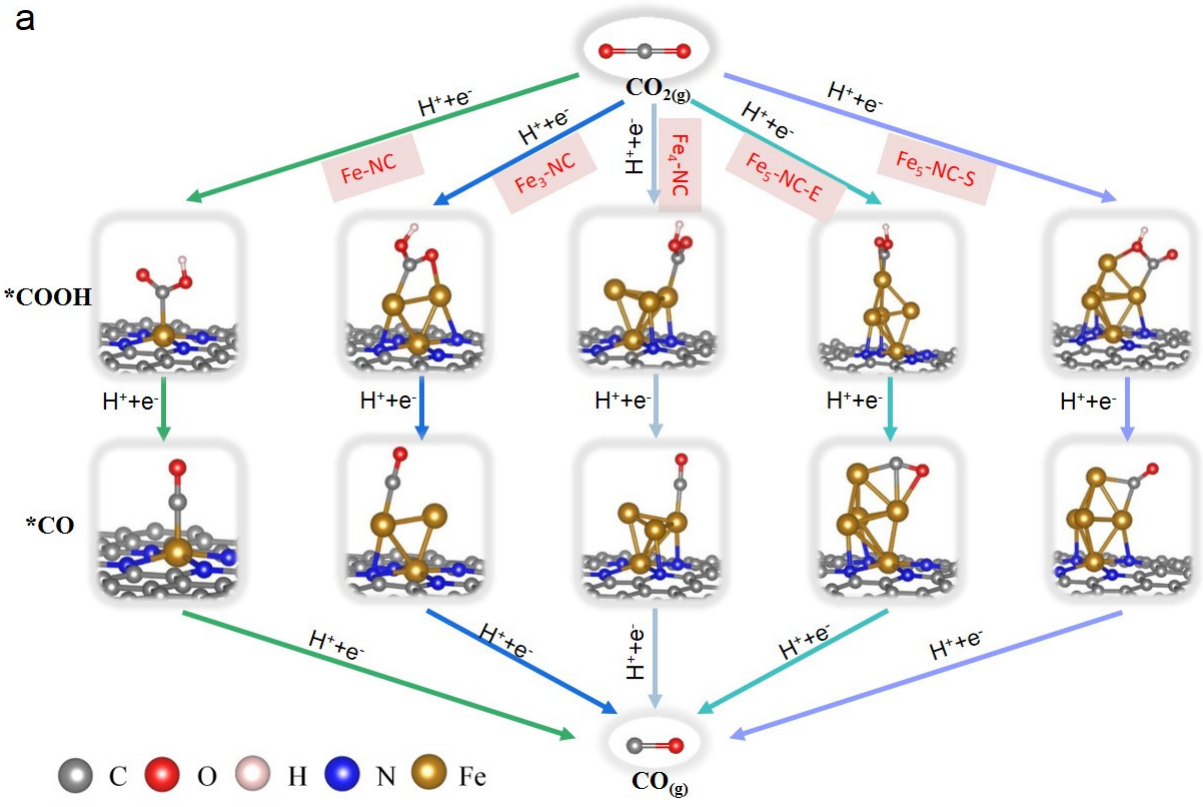

Figure 2. *Cont.*

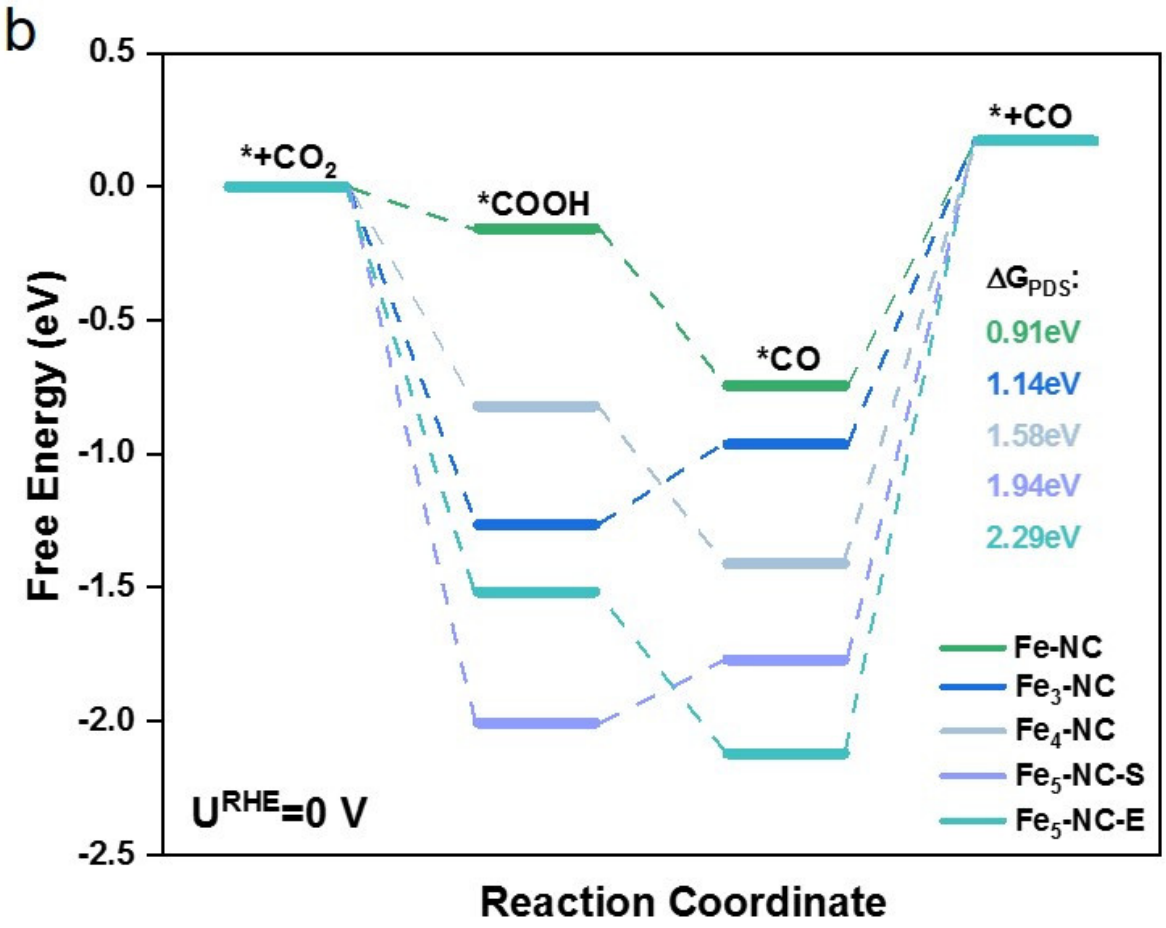

Figure 2. (**a**) The optimized structures of each intermediate during the CO_2 reduction reaction from CO_2 to CO, and (**b**) the Gibbs free energy profiles of CO_2 reduction to CO on Fe_n-NC catalysts during CO_2RR.

Table 2. The Bader charge of Co atoms in Co_5-NC, binding energy (E_b) between the Co_5 cluster and NC and the cohesive energy (E_c) of Co atoms in the Co_5 cluster.

Catalyst	Bader Charge (e)					E_b (eV)	E_c (eV)
	Co ^{1site}	Co ^{2site}	Co ^{3site}	Co ^{4site}	Co ^{5site}		
Co_5-NC	−0.71	−0.34	−0.31	−0.24	0.06	−10.00	−1.39

To further study the mechanisms of CO_2RR catalyzed by Fe_5-NC and Co_5-NC, the optimized structures and the energy profiles along the reaction coordinate for CO_2RR to both C_2H_4 and CH_3CH_2OH on Fe_5-NC and Co_5-NC are calculated as shown in Figures 3 and 4, respectively. It can be found that two strongly adsorbed CO molecules adsorbed on the two adjacent metal atoms through carbon atoms either on the Fe_5 or the Co_5 clusters before the C-C bond formation. The two CO molecules will couple with each other via the top Fe or Co atom in the following steps of CO_2RR. For the CO_2RR on Fe_5-NC, the Gibbs free energy for the hydrogenation of the *CO dimer is uphill with an energy value of 0.79 eV, which is the highest energy during the formation of both C_2H_4 and CH_3CH_2OH. Thus, it can be deemed that the C-C coupling reaction for the CO_2RR from CO_2 to C_2 chemicals is the PDS. Furthermore, it can be speculated that both C_2H_4 and CH_3CH_2OH products can be achieved with Fe_5-NC catalyst, and the amount of C_2H_4 should be much more than the CH_3CH_2OH. Because the Gibbs free energy for the hydrogenation of $*CH_2CHO$ to C_2H_4 is energy thermodynamically favorable, while the hydrogenation of $*CH_2CHO$ to $*CH_3CHO$ is an uphill reaction with a free energy of 0.26 eV.

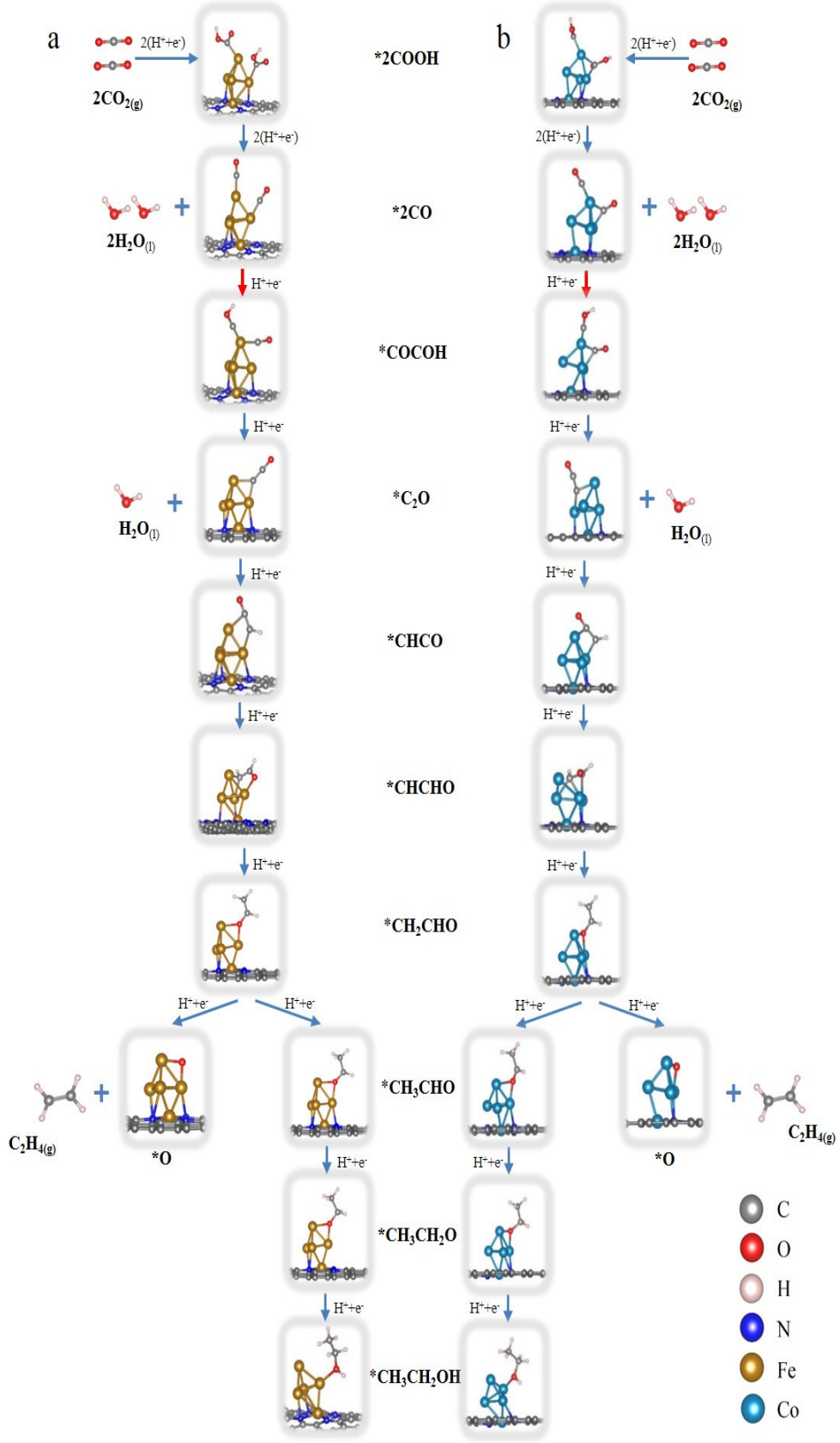

Figure 3. Optimized structures of intermediate Fe_5-NC (**a**) and Co_5-NC catalysts (**b**) during the CO_2RR process.

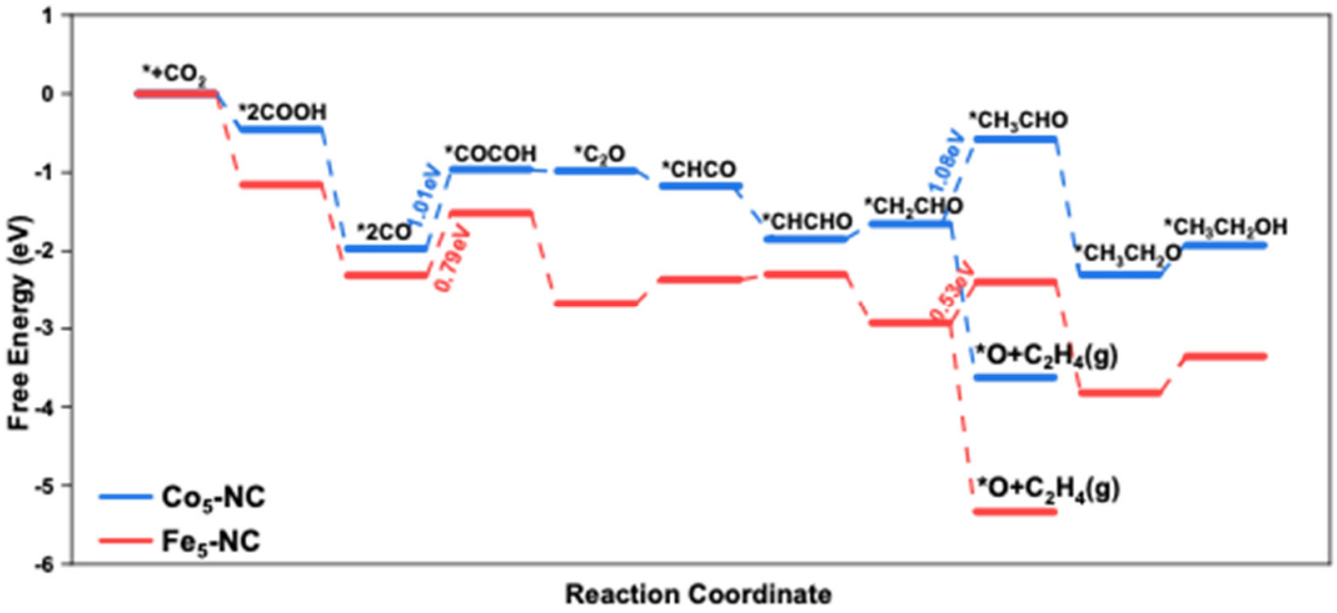

Figure 4. Gibbs free energy profiles for CO_2RR on Fe_5-NC and Co_5-NC.

For the CO_2RR on Co_5-NC, the Gibbs free energy for the hydrogenation of the *CO dimer is uphill with an energy of 1.01 eV, which is 0.22 eV higher than that of the Fe_5-NC. However, the Gibbs free energy for the hydrogenation of *CH_2CHO to *CH_3CHO is (0.07 eV higher) comparable with that in the C-C coupling reaction, which means that the hydrogenation of *CH_2CHO to *CH_3CHO becomes the PDS. Thus, most of the final C_2 products should be C_2H_4. In general, the Fe_5-NC has good catalytic activity towards the C_2 chemicals with relatively lower free energy change (0.53 eV), while the selectivity is not as good as Co_5-NC. However, Co_5-NC possesses better selectivity while the activity is lower than Fe_5-NC.

The d-band center of the TM and its electronic occupancy can affect the bonding strength between the intermediate and the catalytic surface. As shown in Figure 5, the PDOS of Fe *d* orbit from the top- and sub-layer structures show much more differences than that of the Co *d* orbit on Co_5-NC. Furthermore, the d band center of the top Fe atom in the Fe_5 cluster is −3.48 eV, while it becomes −1.59 eV for the sub-layer atoms. However, the d band center of the top Co atom is −1.34 eV, and it only changes to −1.47 eV for the sub-layer atoms. A much bigger discrepancy of the d band center between the top Fe atom and sub-layer atoms than that in the Co_5 cluster may boost the C-C coupling reaction, which could be called the synergy effect between the top- and sub-layer metal atoms. Our findings are consistent with the synergy effect between Cu^+ and Cu^0, and the surface can significantly improve the kinetics and thermodynamics of both CO_2 activation and CO dimerization. Cu metal embedded in an oxidized matrix catalyst can promote CO_2 activation and CO dimerization for electrochemical reduction of CO_2 [41].

Our theoretical calculations found that the multiple active sites in both the Fe_5 and Co_5 cluster-based catalysts facilitate the stabilization of *CO on the catalyst surface and the formation of C-C bonds. Both geometrical effects and electronic effects are the key factors leading to the Fe_5 and Co_5 clusters exhibiting better activity and/or selectivity over the single metal component. Furthermore, the tunable synthesis of Fe and Co alloys supported on NC may promote both their activity and selectivity toward CO_2RR. Therefore, Fe_5, Co_5 and the related tunable alloy clusters show great potential applications in electrocatalytic CO_2RR, and our methods provide a concept for designing the improved CO_2RR electrocatalysts.

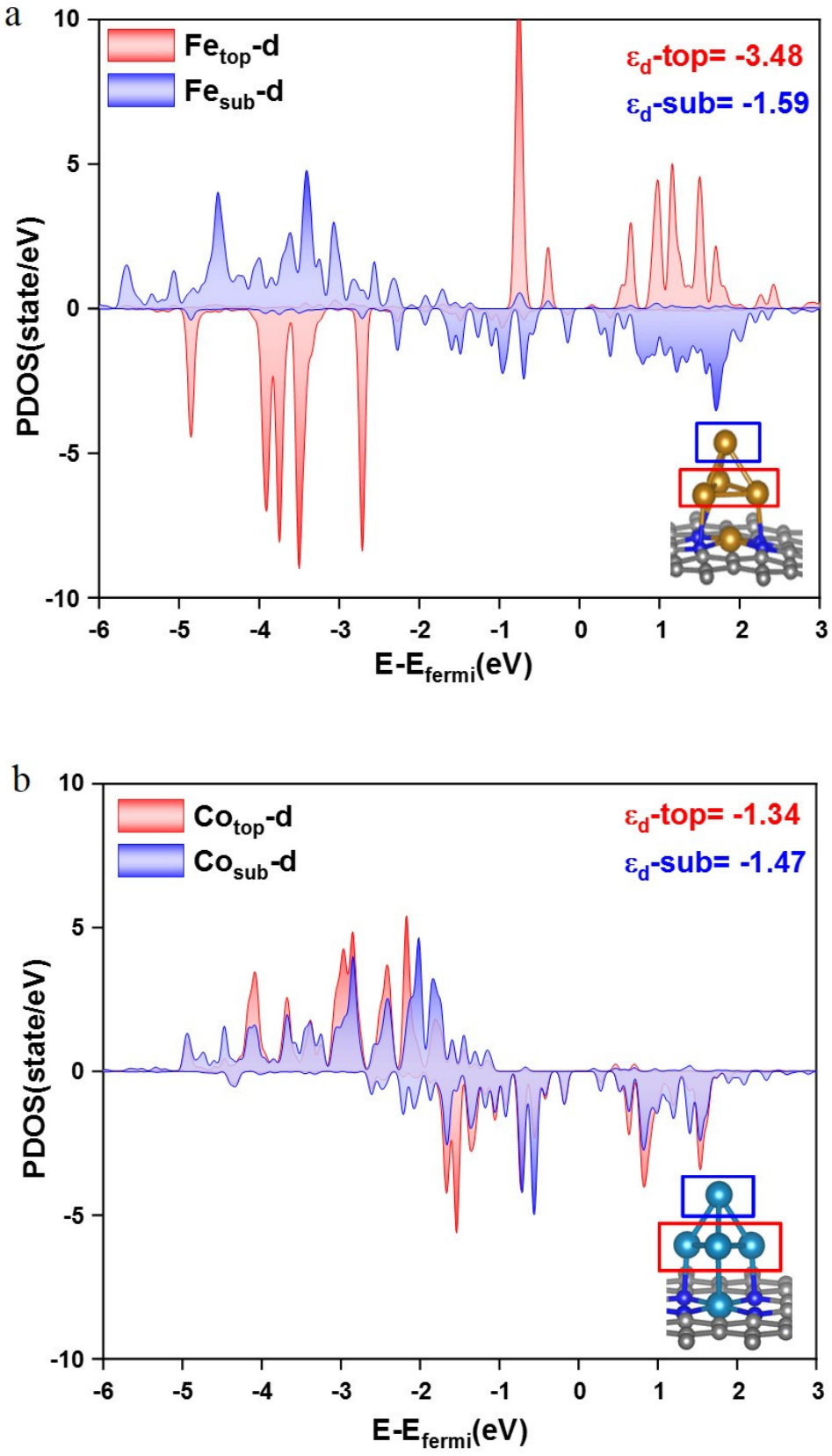

Figure 5. The PDOS of the d orbitals of the single top Fe atom (red) and average three middle Fe atoms (blue) in Fe_5-NC (**a**), and the PDOS of the d orbitals of the single top Co atom (red) and average three middle Co atoms (blue) in Co_5-NC (**b**).

4. Conclusions

The stability of the Fe_n (n = 1, 3, 4, and 5) clusters was studied first, and it can be found that the Fe_n anchors stably on the nitrogen-doped carbon via a basic Fe-NC structure. With the increasing of Fe atoms in the cluster, both the binding energy and cohesive energy become thermodynamically favorable, which means a small cluster tends to aggregate to be a bigger one. While for the Fe_5 cluster, the binding energy decreases because there is no interaction between the topmost Fe atom with the NC support anymore. In addition, the CO desorption is the most difficult on the Fe_5 cluster, which is beneficial to the subsequent reaction products from CO. Hence, the Fe_5-NC cluster was chosen to be studied as our C_2 catalyst, and Co_5-NC was comparatively studied as well. The results show that Fe_5-NC has better activity towards CO_2RR, and the products should be the mixed C_2H_4 and CH_3CH_2OH, since the PDS is the C-C coupling reaction with a free energy change of only 0.79 eV. The free energy change is only 0.53 eV for the reduction of CH_2CHO to CH_3CHO, and the reduction of CH_2CHO to C_2H_4 is a spontaneous step without any free energy change. Considering the fact that C_2H_4 is a gas, Fe_5-NC should be a good catalyst for CO_2RR to liquid ethanol with a relatively lower yield since part of the C_2H_4 gas will also be produced. Furthermore, Co_5-NC possesses a relatively good selectivity, but bad activity since the reduction of CH_2CHO to CH_3CHO is the PDS, and the free energy change is 1.09 eV. The PDOS and d band center analysis demonstrates that the relative energy favorable C-C coupling reaction on the Fe_5 cluster could be attributed to the larger discrepancy of d electrons of the two CO-adsorbing Fe atoms. This paper predicts a good application prospect of TM clusters supported on nitrogen-doped graphene for CO_2RR, and the new insight into the relationship between selectivity and activity sheds light on a new route for understanding and designing highly efficient non-precious catalysts for CO_2RR.

Supplementary Materials: The following supporting information can be downloaded at: https://www.mdpi.com/article/10.3390/nano12132239/s1, Figure S1: The optimized structures of Co_5 supported on four nitrogen doped carbon (NC). Number shown in structures labels the Co atoms.

Author Contributions: Conceptualization, X.Q. and N.Y.; Methodology, N.Y., Q.X. and X.Q.; Software, Q.X., T.Y., Q.Z. and C.F.; Visualization, Q.X. and J.J.; Formal analysis, X.Q., N.Y., and Q.X.; Writing—Original Draft, X.Q. and Q.X.; Writing—Review and Editing, X.Q. and N.Y.; Supervision, X.Q. All authors have read and agreed to the published version of the manuscript.

Funding: This work was supported by the China Postdoctoral Science Foundation (2021M700621), and the 2021 Talent Introduction Project of Chongqing Medical and Pharmaceutical College: ygz2021104.

Data Availability Statement: The data presented in this study are available in this article.

Conflicts of Interest: The authors declare no conflict of interest.

References

1. Birdja, Y.Y.; Pérez-Gallent, E.; Figueiredo, M.C.; Göttle, A.J.; Calle-Vallejo, F.; Koper, M.T.M. Advances and challenges in understanding the electrocatalytic conversion of carbon dioxide to fuels. *Nat. Energy* **2019**, *4*, 732–745. [CrossRef]
2. Wei, X.; Xiao, S.; Wu, R.; Zhu, Z.; Zhao, L.; Li, Z.; Wang, J.; Chen, J.S.; Wei, Z. Activating COOH* intermediate by $Ni/Ni_3ZnC_{0.7}$ heterostructure in porous N-doped carbon nanofibers for boosting CO_2 electroreduction. *Appl. Catal. B Environ.* **2022**, *302*, 120861. [CrossRef]
3. Li, Z.; Wu, R.; Xiao, S.; Yang, Y.; Lai, L.; Chen, J.S.; Chen, Y. Axial chlorine coordinated iron-nitrogen-carbon single-atom catalysts for efficient electrochemical CO_2 reduction. *Chem. Eng. J.* **2022**, *430*, 132882. [CrossRef]
4. Lu, S.; Wang, Y.; Xiang, H.; Lei, H.; Xu, B.B.; Xing, L.; Yu, E.H.; Liu, T.X. Mass transfer effect to electrochemical reduction of CO_2: Electrode, electrocatalyst and electrolyte. *J. Energy Storage* **2022**, *52*, 104764. [CrossRef]
5. Wu, Y.; Jiang, Z.; Lu, X.; Liang, Y.; Wang, H. Domino electroreduction of CO_2 to methanol on a molecular catalyst. *Nature* **2019**, *575*, 639–642. [CrossRef] [PubMed]
6. Wang, Y.; Ngoc Pham, T.; Tian, Y.; Morikawa, Y.; Yan, L. Density functional theory study on a nitrogen-rich carbon nitride material C_3N_5 as photocatalyst for CO_2 reduction to C1 and C2 products. *J. Colloid Interface Sci.* **2021**, *585*, 740–749. [CrossRef] [PubMed]
7. Xiao, C.; Zhang, J. Architectural Design for Enhanced C_2 Product Selectivity in Electrochemical CO_2 Reduction Using Cu-Based Catalysts: A Review. *ACS Nano* **2021**, *15*, 7975–8000. [CrossRef]

8. Wang, Y.; Lei, H.; Lu, S.; Yang, Z.; Xu, B.B.; Xing, L.; Liu, T.X. Cu_2O nano-flowers/graphene enabled scaffolding structure catalyst layer for enhanced CO_2 electrochemical reduction. *Appl. Catal. B Environ.* **2022**, *305*, 121022. [CrossRef]
9. Lu, Q.; Rosen, J.; Jiao, F. Nanostructured Metallic Electrocatalysts for Carbon Dioxide Reduction. *ChemCatChem* **2015**, *7*, 38–47. [CrossRef]
10. Mistry, H.; Choi, Y.W.; Bagger, A.; Scholten, F.; Bonifacio, C.S.; Sinev, I.; Divins, N.J.; Zegkinoglou, I.; Jeon, H.S.; Kisslinger, K.; et al. Enhanced Carbon Dioxide Electroreduction to Carbon Monoxide over Defect-Rich Plasma-Activated Silver Catalysts. *Angew. Chem. Int. Ed. Engl.* **2017**, *56*, 11394–11398. [CrossRef]
11. Chen, Y.; Li, C.W.; Kanan, M.W. Aqueous CO_2 reduction at very low overpotential on oxide-derived Au nanoparticles. *J. Am. Chem. Soc.* **2012**, *134*, 19969–19972. [CrossRef] [PubMed]
12. Zhu, W.; Michalsky, R.; Metin, O.; Lv, H.; Guo, S.; Wright, C.J.; Sun, X.; Peterson, A.A.; Sun, S. Monodisperse Au nanoparticles for selective electrocatalytic reduction of CO_2 to CO. *J. Am. Chem. Soc.* **2013**, *135*, 16833–16836. [CrossRef] [PubMed]
13. Mistry, H.; Reske, R.; Zeng, Z.; Zhao, Z.J.; Greeley, J.; Strasser, P.; Cuenya, B.R. Exceptional size-dependent activity enhancement in the electroreduction of CO_2 over Au nanoparticles. *J. Am. Chem. Soc.* **2014**, *136*, 16473–16476. [CrossRef] [PubMed]
14. Ju, W.; Bagger, A.; Hao, G.P.; Varela, A.S.; Sinev, I.; Bon, V.; Roldan Cuenya, B.; Kaskel, S.; Rossmeisl, J.; Strasser, P. Understanding activity and selectivity of metal-nitrogen-doped carbon catalysts for electrochemical reduction of CO_2. *Nat. Commun.* **2017**, *8*, 944. [CrossRef]
15. Bagger, A.; Ju, W.; Varela, A.S.; Strasser, P.; Rossmeisl, J. Single site porphyrine-like structures advantages over metals for selective electrochemical CO_2 reduction. *Catal. Today* **2017**, *288*, 74–78. [CrossRef]
16. Zu, X.; Li, X.; Liu, W.; Sun, Y.; Xu, J.; Yao, T.; Yan, W.; Gao, S.; Wang, C.; Wei, S.; et al. Efficient and Robust Carbon Dioxide Electroreduction Enabled by Atomically Dispersed $Sn^{\delta+}$ Sites. *Adv. Mater.* **2019**, *31*, e1808135. [CrossRef]
17. Gao, D.; Arán-Ais, R.M.; Jeon, H.S.; Roldan Cuenya, B. Rational catalyst and electrolyte design for CO_2 electroreduction towards multicarbon products. *Nat. Catal.* **2019**, *2*, 198–210. [CrossRef]
18. Cheng, M.J.; Clark, E.L.; Pham, H.H.; Bell, A.T.; Head-Gordon, M. Quantum Mechanical Screening of Single-Atom Bimetallic Alloys for the Selective Reduction of CO_2 to C_1 Hydrocarbons. *ACS Catal.* **2016**, *6*, 7769–7777. [CrossRef]
19. Prieto, G. Carbon Dioxide Hydrogenation into Higher Hydrocarbons and Oxygenates: Thermodynamic and Kinetic Bounds and Progress with Heterogeneous and Homogeneous Catalysis. *ChemSusChem* **2017**, *10*, 1056–1070. [CrossRef]
20. Alvarez, A.; Bansode, A.; Urakawa, A.; Bavykina, A.V.; Wezendonk, T.A.; Makkee, M.; Gascon, J.; Kapteijn, F. Challenges in the Greener Production of Formates/Formic Acid, Methanol, and DME by Heterogeneously Catalyzed CO_2 Hydrogenation Processes. *Chem. Rev.* **2017**, *117*, 9804–9838. [CrossRef]
21. Jiang, K.; Sandberg, R.B.; Akey, A.J.; Liu, X.; Bell, D.C.; Nørskov, J.K.; Chan, K.; Wang, H. Metal ion cycling of Cu foil for selective C–C coupling in electrochemical CO_2 reduction. *Nat. Catal.* **2018**, *1*, 111–119. [CrossRef]
22. Li, X.; Yu, J.; Jaroniec, M.; Chen, X. Cocatalysts for Selective Photoreduction of CO_2 into Solar Fuels. *Chem. Rev.* **2019**, *119*, 3962–4179. [CrossRef] [PubMed]
23. Ross, M.B.; De Luna, P.; Li, Y.F.; Dinh, C.-T.; Kim, D.; Yang, P.; Sargent, E.H. Designing materials for electrochemical carbon dioxide recycling. *Nat. Catal.* **2019**, *2*, 648–658. [CrossRef]
24. Karapinar, D.; Huan, N.T.; Ranjbar Sahraie, N.; Li, J.; Wakerley, D.; Touati, N.; Zanna, S.; Taverna, D.; Galvao Tizei, L.H.; Zitolo, A.; et al. Electroreduction of CO_2 on Single-Site Copper-Nitrogen-Doped Carbon Material: Selective Formation of Ethanol and Reversible Restructuration of the Metal Sites. *Angew. Chem. Int. Ed. Engl.* **2019**, *58*, 15098–15103. [CrossRef]
25. Zhu, Y.; Yang, X.; Peng, C.; Priest, C.; Mei, Y.; Wu, G. Carbon-Supported Single Metal Site Catalysts for Electrochemical CO_2 Reduction to CO and Beyond. *Small* **2021**, *17*, e2005148. [CrossRef]
26. Imaoka, T.; Akanuma, Y.; Haruta, N.; Tsuchiya, S.; Ishihara, K.; Okayasu, T.; Chun, W.J.; Takahashi, M.; Yamamoto, K. Platinum clusters with precise numbers of atoms for preparative-scale catalysis. *Nat. Commun.* **2017**, *8*, 688. [CrossRef]
27. Xu, J.; Li, R.; Zeng, R.; Li, Y.; Pan, Q.; Zhong, H.; Chen, J. Underpotential deposition of Cu clusters on sulfur and nitrogen Co-doped graphite foam for the oxygen reduction reaction. *ChemElectroChem* **2019**, *6*, 5682–5687. [CrossRef]
28. Pei, W.; Zhou, S.; Zhao, J.; Xu, X.; Du, Y.; Dou, S.X. Immobilized trimeric metal clusters: A family of the smallest catalysts for selective CO_2 reduction toward multi-carbon products. *Nano Energy* **2020**, *76*, 105049. [CrossRef]
29. Kresse, G.; Furthmiiller, J. Efficiency of ab-initio total energy calculations for metals and semiconductors using a plane-wave basis set. *Comput. Mater. Sci.* **1996**, *6*, 15–50. [CrossRef]
30. Blochl, P.E. Projector augmented-wave method. *Phys. Rev. B Condens. Matter.* **1994**, *50*, 17953–17979. [CrossRef]
31. Kresse, G.; Furthmiiller, J. From ultrasoft pseudopotentials to the projector augmented-wave method. *Phys. Rev. B Condens. Matter.* **1999**, *59*, 1758–1775. [CrossRef]
32. Perdew, J.P.; Burke, K.; Ernzerhof, M. Generalized Gradient Approximation Made Simple. *Phys. Rev. Lett.* **1996**, *77*, 3865–3868. [CrossRef] [PubMed]
33. Monkhorst, H.J.; Pack, J.D. Special points for Brillouin-zone integrations. *Phys. Rev. B* **1976**, *13*, 5188–5192. [CrossRef]
34. Nørskov, J.K.; Rossmeisl, J.; Logadottir, A.; Lindqvist, L.; Kitchin, J.R.; Bligaard, T.; Jónsson, H. Origin of the Overpotential for Oxygen Reduction at a Fuel-Cell Cathode. *J. Phys. Chem. B* **2004**, *108*, 17886–17892. [CrossRef]
35. Rossmeisl, J.; Logadottir, A.; Nørskov, J.K. Electrolysis of water on (oxidized) metal surfaces. *Chem. Phys.* **2005**, *319*, 178–184. [CrossRef]

36. Peterson, A.A.; Abild-Pedersen, F.; Felix Studt, F.; Rossmeisl, J.; Nørskov, J.K. How copper catalyzes the electroreduction of carbon dioxide into hydrocarbon fuels. *Energy Environ. Sci.* **2010**, *3*, 1311–1315. [CrossRef]
37. Wang, Y.; Yuan, H.; Li, Y.; Chen, Z. Two-dimensional iron-phthalocyanine (Fe-Pc) monolayer as a promising single-atom-catalyst for oxygen reduction reaction: A computational study. *Nanoscale* **2015**, *7*, 11633–11641. [CrossRef]
38. Lim, D.H.; Wilcox, J. Mechanisms of the Oxygen Reduction Reaction on Defective Graphene-Supported Pt Nanoparticles from First-Principles. *J. Phys. Chem. C* **2012**, *116*, 3653–3660. [CrossRef]
39. Cui, C.; Zhang, H.; Luo, Z. Nitrogen reduction reaction on small iron clusters supported by N-doped graphene: A theoretical study of the atomically precise active-site mechanism. *Nano Res.* **2020**, *13*, 2280–2288. [CrossRef]
40. Li, X.F.; Li, Q.K.; Cheng, J.; Liu, L.; Yan, Q.; Wu, Y.; Zhang, X.H.; Wang, Z.Y.; Qiu, Q.; Luo, Y. Conversion of Dinitrogen to Ammonia by FeN_3-Embedded Graphene. *J. Am. Chem. Soc.* **2016**, *138*, 8706–8709. [CrossRef]
41. Xiao, H.; Goddard, W.A., 3rd; Cheng, T.; Liu, Y. Cu metal embedded in oxidized matrix catalyst to promote CO_2 activation and CO dimerization for electrochemical reduction of CO_2. *Proc. Natl. Acad. Sci. USA* **2017**, *114*, 6685–6688. [CrossRef] [PubMed]
42. Zhou, Y.; Che, F.; Liu, M.; Zou, C.; Liang, Z.; De Luna, P.; Yuan, H.; Li, J.; Wang, Z.; Xie, H.; et al. Dopant-induced electron localization drives CO_2 reduction to C_2 hydrocarbons. *Nat. Chem.* **2018**, *10*, 974–980. [CrossRef] [PubMed]
43. Chen, S.; Wang, B.; Zhu, J.; Wang, L.; Ou, H.; Zhang, Z.; Liang, X.; Zheng, L.; Zhou, L.; Su, Y.Q.; et al. Lewis Acid Site-Promoted Single-Atomic Cu Catalyzes Electrochemical CO_2 Methanation. *Nano Lett.* **2021**, *21*, 7325–7331. [CrossRef] [PubMed]
44. Varela, A.S.; Ranjbar Sahraie, N.; Steinberg, J.; Ju, W.; Oh, H.S.; Strasser, P. Metal-Doped Nitrogenated Carbon as an Efficient Catalyst for Direct CO_2 Electroreduction to CO and Hydrocarbons. *Angew. Chem Int. Ed. Engl.* **2015**, *54*, 10758–10762. [CrossRef] [PubMed]